Bima Journal of Science and Technology, Vol. 8(1B) Apr, 2024 ISSN: 2536-6041

DOI: 10.56892/bima.v8i1.636

First-Principles Study of Electronic and Nonlinear Optical Properties of Halides and Rubidium Halides Substituted Anthracene Diimide

Njapba S. Augustine[1]* and Buba Barsisa[2]

[1]Department of Physics, Gombe State University, PMB 127, Gombe State, Nigeria

Corresponding Author: augustinenjapba@gsu.edu.ng

ABSTRACT

This study reports the density functional theory calculations of UV-Visible, HOMO-LUMO energy band gap as measure of reactivity, nonlinear optical properties and natural bond orbital properties of novel Anthracene diimide derivatives. The UV-Visible absorption peak resulting from electronic transitions HOMO-LUMO observed to be the highest among others for ADI-Rb_2I_2 occurs at 77.94 nm is also in good agreement with the experimental value. The HOMO-LUMO energy band gap has been found to be reasonably small ≈ 0.54 eV. The total frequency-dependent polarizability for RHF method is remarkably positive and far greater than the values obtained using B3LYP functional. This variation in the total frequency-dependent polarizability is due to the sensitivity of the nonlinear optical property to the functional. Our calculation of total static first order hyperpolarizability with RHF method and B3LYP functional are approximately 1.9, 28, 73, 161, 2309, 0.08, 26, 35, 44, 53, 114, and 454 many times greater than the standard compound Urea. These results indicate that Anthracene diimide substituted halides and rubidium halides are suitable for nonlinear optical applications. Natural bond orbital analysis reveals that donor LP (3) $O_{22}\rightarrow\pi^*(N_{24}\text{-}C_{28})$ acceptor interactions corresponds to the highest second order perturbation energy E_2 = 111.11 kcal/mol associated with electron delocalization.

Keywords: DFT, LUMO energy, Anthracene diimide, polarizability, First order hyperpolarizability and delocalization.

INTRODUCTION

Organic semiconductor materials have emerged of recent as a new class of materials with superior remarkable properties that has led to impressive improvement in high performance of novel electronic and optoelectronic devices far greater than the already dominated Si-based semiconductor. This enormous technological progress is driven by its outstanding promising features such as excellent mechanical flexibility, ease of processing, low cost, light weight and large area coverage. This combination of properties has fueled research and development in organic semiconductors in both academic and industry. Organic semiconductors are carbon-based molecules characterized by π -conjugation of the electron system, a very key element responsible for the electronic and optical behavior of organic materials. The π -electrons are delocalized and have the ability to move freely within the chain. It is this property that is responsible for charge-carrier transport within π -conjugated organic based semiconductors. Coropceanu *et al*, (2007) reported that the atomic structure of π -conjugated organic molecules is influential to charge-carrier transport. The delocalization of the π -conjugated framework provides the foundation for a molecular architecture with the possession of an impeccable stability and rich electronic behavior. The appearance of delocalized π - orbitals within the molecule led to the lowest unoccupied molecular orbital (LUMO) and the highest occupied molecular orbital (HOMO). This LUMO and HOMO could be related to the valence band and conduction band in inorganic semiconductors.

DOI: 10.56892/bima.v8i1.636

The LUMO- HOMO energy difference between these molecular orbitals makes them behave as a semiconductor. Semiconducting materials are known for their propagation of electron processes upon light absorption. The conducting properties of an organic semiconductor are dependent on this energy difference that is called the band gap energy (E_g) that lies in the range of 1.2 to 3.5 eV relative to traditional elemental semiconductor, Si with 1.2 eV and Ge 0.76 eV.(Yon *et al*, 2010). π -conjugated organic molecules exhibiting semiconducting properties have their conductivity lies between insulators and conductors in the range 10^{-9} to 10^{-3} / Ωcm .But one of the superiority character of organic molecules is the enhancement of conductivity. This is achieved through the process of doping or substitution. As concerning doping, these materials could be n-type or p-type organic semiconductors. They are of interest because of its unique optical and optoelectronic properties that has enabled the fabrication of new optoelectronic devices having unique functionalities. The physical properties such as optical, charge carrier mobility, HOMO-LUMO levels and structural ordering are tuned by various chemical functionalities. The idea of fine tuning this property of organic materials through either substitution or functionalization gives molecules and molecular materials much promise as building blocks for electronics and optoelectronic devices.

Organic-based semiconductors have various applications in key components of electronic and optoelectronic devices such as organic field effect transistors, organic photovoltaic and organic light-emitting diodes. Common organic semiconductor materials include polycyclic aromatic hydrocarbon, metal complexes and small compounds derived from conducting polymers such as polyacenes, polyphenylamine and polythiophenes. The molecular weight structure and semiconductor properties of these materials have been of great interest in recent years (Liu *et al*, 2021). Also, various aromatic and heteroaromatic cores have been utilized in the development of organic semiconductor. For example, π -conjugated Oligocene (i.e linearly fused-benzene core) represent high performance organic semiconductors for OFET application and thiophene a representative heteroaromatic core, has been widely utilized both for molecular and polymer semiconductor (Numi *et al*, 2012).Moreover, end-side functionalized organic materials such as various imides and core (imides-nitrogen substituent, F, Cl, Br, CN, etc) of Oligocene, i.e. Anthracene, perylene, coronene, benzene, naphthalene, terrylene alternating thiophene based copolymer, polytriphenylamines and dinaphthienothiophenes are of profound interest for the present day fabrication of OFETs, and OTFTs for better performance. Lazaar *et al,* (2020) reported that slight chemical modification of organic molecules such as changing the location of a heteroatom, introducing different substituent and alternative π -conjugated cores change their optical and electrochemical behavior. PDI and NDI are very important useful members of the Oligocene family that are reported to exhibit good n-channel and ambipolar semiconducting properties in OTFTs. One of the early reports of an air-stable n-channel OTFT was demonstrated on a NDI-based semiconductor with Fluorinated alkyl chains. PDI-based semiconductor has been shown as crystalline acceptor in association with electron-donating hexa-peri-hexabenzocoronene to build photovoltaic device with remarkable high quantum efficiencies.

However, to the best of our knowledge, π -conjugated homologous series of the diimide and particularly Anthracene tetracarboxylic diimide, there are very few reports on Anthracene tetracarboxylic diimide (ADI) (Mohebbi *et al,* 2011). ADI is highly a π -

DOI: 10.56892/bima.v8i1.636

conjugated organic molecule, an acene and with a rigid planar linear molecular structure. As a member of the homologous series of diimide, it is an n-type organic semiconductor with high electron affinity, high mobility and excellent stability with potential application as an active element in molecular organics and optoelectronic devices such as OLED and OFETs (Mohebbi *et al*, 2011; Kukhta *et al*, 2008; Yongfang, 2015; Raghunath *et al*, 2006). The Imide is a functional group which contributes a lot to forming high performance n-type molecules. It has a strong electron-withdrawing capability. Usta *et al*, (2012) have studied and fully synthesized and characterized new ADI based N.N'-dialkyl-2, 3, 6,7 Anthracene tetracarboxylic diimide. The synthesis and characterization of new ADI are functionalized with electron-withdrawing groups such as Br, CN, n-Octyl (n-C_8H_{17}), 1H, 1H- perfluorobutyl (-n-CH_2-C_3F_7) substituent in its new structure. The results revealed that the absorption spectra of the π -conjugated based diimide exhibit a maxima in the range of 418 - 436 nm corresponding to transitions of the ADI core with blue-shift in the visible region of the optical spectra. The HOMO and LUMO energies of the new ADI are observed to span a wide range up to 1.0 eV. Mohebbi *et al*, (2011) have reported the synthesis and characterization of Anthracene 1,3, 7, 9 diimide. The HOMO-LUMO energy gap (E_g) calculated is about 2.45 eV. Tyson *et al*, (2008) reported the synthesis and characterization of novel ADI that is prepared from Anthracene dianhydride and triaryl amine-terminated diimide. Li *et al*, (2014) have observed that all electron withdrawing groups attached onto π -conjugated skeleton of the acene improves processability and stability. Wang *et al*, (2007; 2012) reported the only example of OFET based on -2, 3, 6, 7 Anthracene tetracarboxylic diimide as well as is an active layer in n-channel OFET devices.

Despite the research activities on Anthracene diimide π -conjugated organic semiconductor, the development of organic molecular materials for practical application in the field of nonlinear optics has been limited especially when substituted with halides and rubidium halides. Based on this fact, we wish to investigate the electronic and nonlinear optical properties of novel Anthracene diimide organic semiconductor from first principles. Herein, calculations of the electronic and nonlinear optical properties of halides (F_2, Cl_2, Br_2, and I_2) and Rubidium halides (RbF, RbCl, RbBr and RbI) substituted Anthracene diimide using First principles density functional theory (DFT) and time-dependent density functional theory (TD-DFT) study in conjunction with Lanl2dz basis sets are carried out. Theoretical quantum mechanical methods have proven to be useful tools in obtaining the characteristic properties of novel ADI based organic semiconductor in the gas phase.

Theoretical Framework

DFT and TD-DFT are two approaches we will adopt to calculate the properties of novel ADI substituted halides and rubidium halides at end-sides positions on the Anthracene core. These approaches though closely related in principle, yet are mutually exclusive in practice. Both DFT and TD-DFT are implemented in Gaussian 09W program and in many other programs. We will briefly discuss the theory of each method as applicable to the calculation of the properties of novel ADI substituted halides and rubidium structures.

DFT is remarkably popular and less demanding computationally than the CI, MP2 and HF methods (Alkins and Friedman, 2005; Casida, 2009). DFT is based on the theories of Hohenberg and Kohn, Kohn and Shaw where they stated that the total electronic energy of an atom, molecule or ion and other observable material properties are functional of the ground state electronic density, ρ (Hohenberg and

DOI: 10.56892/bima.v8i1.636

Kohn, 1964; Kohn and Shaw, 1965). Expressing this as a mathematical equation we can write

$$E_{TOT}[\rho] = E_T[\rho] + E_V[\rho] + E_J[\rho] + E_{XC}[\rho] \quad (1)$$

In a similar manner, the Kohn-Shaw equation for single-particle non-interacting Schrodinger equation of interest is expressed as

$$\overline{H}(r)\psi(r) = \left[-\frac{\nabla^2}{2} + V_s(r)\right]\psi(r) = E_i\psi(r) \quad (2)$$

where

$$V_s(r) = V_{ext}(r) + \int \frac{\rho(r)}{|r - r^1|} dr^1 + V_{xc}(r) \quad (3)$$

And

$$\rho(r) = \sum_{i=1}^{N} |\psi(r)|^2 \quad (4)$$

$$V_{XC}[\rho](r) = \frac{\partial E_{XC}|\rho|}{\partial \rho(r)} \quad (5)$$

Equations 2, 3, and 4 constitute the ground state Kohn-Shaw equations. Since no exact form of the exchange correlation XC functional is known, this functional is approximated in practice. Once an XC approximation is chosen, the equations are solved self-consistently.

Time-dependent density functional theory (TD-DFT) is an extension of the classical DFT into the time domain to handle time-dependent cases. DFT is a static ground-state theory that cannot compute time-dependent phenomena like excited states of molecules and others. TD-DFT seek to improve the ground-state DFT to compute the static properties of atoms and molecules such as transition frequency, oscillator strength, the calculation of photoabsorption spectra and more generally the interaction of electromagnetic fields with matter(Marques and Gross, 2004). Using TD-DFT, system with time-dependent potential can be treated. It is flexible, simple accurate powerful method for calculating nonlinear parameters of materials like dipole moment, polarizability, hyperpolarizability, excitation states and many other properties (Casida, 1995; Ataf *et al*, 2018; Ding *et al*, 2013).The foundation of TD-DFT was established by Runge and Gross (Runge and Gross, 1984).

For a monochromatic electric field, the equation of the time-dependent dipole moment can be expanded in Taylor series (Ding *et al*, 2013; Reis *et al*, 1998).

$$\mu(t) = \mu_i^o + \sum_1 \int_{-\infty}^{\infty} dt_1 \alpha_{ij}(t - t_1) E_i(t_1) + \frac{1}{21} \sum_{jk} \iint_{-\infty} dt_1 dt_2 \beta_{ijk}(t - t_1, t - t_2) E_j(t_1) E_k(t_2)$$
$$+ \frac{1}{31} \sum_{jkl} \iiint_{-\infty} dt_1 dt_2 dt_3 \gamma_{ijkl}(t - t_1, t - t_2, t - t_3) E_i(t_1) E_k(t_2) E_l(t_3) \quad (6)$$

DOI: 10.56892/bima.v8i1.636

where i, j, k are Cartesian coordinates x, y, z . μ_i^o is the permanent dipole moment in the absence of an external electric field. $\alpha(t-t_1)$, $\beta(t-t_1,t-t_2)$, and $\gamma(t-t_1,t-t_2,t-t_3)$ are time domain response functions of first, second and third order respectively also the frequency-dependent polarizability and hyperpolarizability. To evaluate these values for a time-dependent external monochromatic field E (t), suppose that (Bulik *et al*, 2013).

$$E(t) = A\cos(\omega t) \tag{7}$$

In the presence of time-dependent field, E (t), substitute this equation into equation (6), we have

$$\mu(t) = \mu_i^o + \sum_i \alpha_{ij}(-\omega;\omega) A\cos\omega t + \frac{1}{4}\sum_{jk}\{\beta_{ijk}(-2\omega;\omega,\omega)\cos 2\omega t + \beta_{ijk}(0;\omega,\omega)A_1A_2\} + \\ + \frac{1}{24}\sum_{jkl}\{\gamma_{ijkl}(-3\omega;\omega,\omega,\omega)\cos 3\omega t + 3\gamma_{ijkl}(-\omega;\omega,\omega,\omega)A_1A_2A_3\} \tag{8}$$

where $\alpha(-\omega,\omega)$ is the frequency-dependent polarizability, $\beta(-2\omega;\omega,\omega)$ and $\beta(0;\omega,\omega)$ are the frequency-dependent first-order hyperpolarizability, $\gamma(-3\omega;\omega,\omega,\omega)$ and $\gamma(-\omega;\omega,\omega,\omega)$ are the frequency-dependent second-order hyperpolarizability respectively. Equation (8) provides the fundamental origin of non-linearities at the microscopic level, i.e. different values of the optical frequencies giving rise to different nonlinear optical phenomena. When all the optical frequencies are zero, these terms are identical to the static polarizability i.e. first and second hyperpolarizability $\alpha_{i,j}$, $\beta_{i,j,k}$, and $\gamma_{i,j,k,l}$ such that $\alpha(0;0) = \alpha$, $\beta(0;0,0) = \beta$,and $\gamma(0;0,0,0,) = \gamma$ Similarly for a dynamic case or frequency-dependent the optical frequency is not zero i.e. we have, $\alpha(-\omega;\omega) = \alpha(\omega)$, $\beta(-\omega;\omega,0)$, or $\beta(0;\omega,-\omega)$ and $\beta(-2\omega;\omega,\omega)$ respectively. In this work, the dynamic polarizability $\alpha(\omega)$ and first order hyperpolarizability $\beta(-\omega;\omega,0)$, are tensor components that are calculated at an optical field frequency of 0.02389 a.u. using the coupled-perturbed Hartree-Fock (CPHF) method as implemented in 09 Gaussian program package. The output from Gaussian 09 package provides 10 components of this matrix as $\beta_{xxx}, \beta_{xxy}, \beta_{xyy}, \beta_{yyy}, \beta_{xxz}, \beta_{xyz}, \beta_{yyz}, \beta_{xzz}, \beta_{yzz}, \beta_{zzz}$ respectively. These parameters are computed for both static and frequency-dependence using first principle based approach with TD-DFT at B3PW91 functional and LANL2DZ basis sets. As usual for TD-DFT calculations, the accuracy of these electronic transitions is ± 0.3 eV.

COMPUTATIONAL METHODOLOGY

All DFT and TD-DFT calculations were performed with Gaussian 09 program package and visualized with GaussView 5.0.8 version in conjunction with B3PW91 functional and LANL2DZ basis sets (Frisch, 1996). The structural optimization of the molecular structure was carried out without symmetry constraint using pure B3PW91 functional in the gas phase. Positive vibrational frequencies confirmed the stability of the optimized molecular geometries of novel Anthracene diimide substituted halides and rubidium halides respectively. All molecular geometries are planar with C_1 symmetry. Figure 1 shows the molecules studied by employing first principle approach. The molecular structures of our novel Anthracene diimide substituted

DOI: 10.56892/bima.v8i1.636

halides and rubidium halides are all restricted at this given functional. All energies and molecular orbitals were obtained by single-point calculations. Frequency-dependent linear polarizability and first-order hyperpolarizability are obtained from Gaussian 09 package. and from many other programs as well. These nonlinear optical parameters employ standard Gaussian 09 keyword 'polar' and CPHF code for the calculation of dynamic polarizability and hyperpolarizability. This keyword used means the nonlinear parameters were obtained analytically rather than by numerical differentiation. For comparison purpose, HF method is employed to investigate the nonlinear optical parameters at the same level of theory and basis sets. The HOMO-LUMO energy gap E_g, of the novel Anthracene diimide derivatives were calculated as follows:

$$E_g = E_{LUMO} - E_{HOMO} \qquad (9)$$

The E_{LUMO} and E_{HOMO} energies represent the energies of the lowest unoccupied and highest occupied molecular orbitals respectively. The ultra-violet spectra (UV-vis) were calculated by solving the TD-DFT equation approach. The natural bond orbitals (NBO) analysis was carried out at the same level of theory and basis sets.

These nonlinear optical properties were calculated using the following equations. The dipole moment was obtained from

$$\mu^2 = \mu_x^2 + \mu_y^2 + \mu_z^2 \qquad (10)$$

The mean polarizability was from the components

$$\langle \alpha \rangle = \frac{1}{3}\left[\alpha_{xx} + \alpha_{yy} + \alpha_{zz} \right] \qquad (11)$$

The complete equation for calculating the magnitude of β , the first order hyperpolarizability from Gaussian 09 output is given as follows:

$$\beta_{tot} = \left[\left(\beta_{xxx} + \beta_{xyy} + \beta_{xzz} \right)^2 + \left(\beta_{yyy} + \beta_{yxx} + \beta_{yzz} \right)^2 + \left(\beta_{zzz} + \beta_{zxx} + \beta_{zyy} \right)^2 \right]^{\frac{1}{2}} \qquad (12)$$

The nonlinear optical parameters were calculated using the optical field frequency $\omega = 0.023890$ a.u. Since these tensor values of the output file from Gaussian 09 are reported in atomic units (a.u.) , the calculated values were converted into electrostatic units(for α : 1 a.u.= 0.1482 x 10^{-24} esu, for β : 1 a.u.= 8.6393 x 10^{-33} esu).

Bima Journal of Science and Technology, Vol. 8(1B) Apr, 2024 ISSN: 2536-6041

DOI: 10.56892/bima.v8i1.636

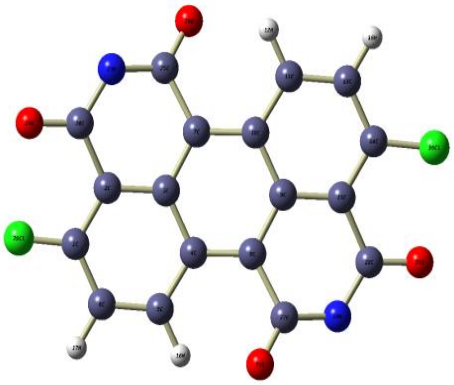

(a)ADI-Cl_2

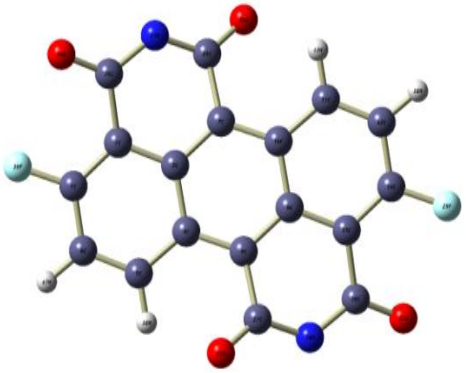

(b)ADI-F_2 b

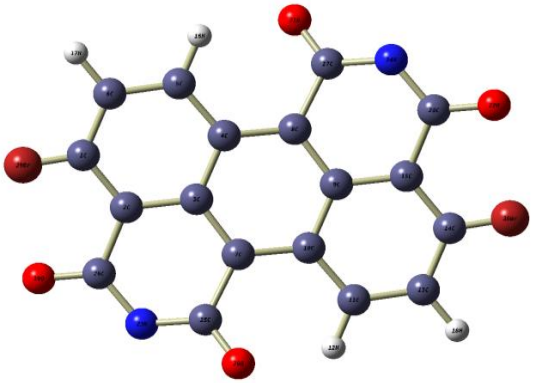

(c) ADI-Br_2

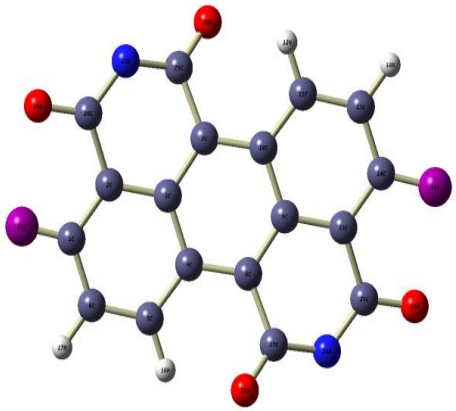

(d) ADI-I_2

Figure 1: Optimized Structures ADI-F_2, ADI-Cl_2, ADI-Br_2 and ADI-I_2 of novel Anthracene diimide Substituted Halides used in the study.

RESULTS AND DISCUSSION

Natural Bond Orbital

The natural bond orbital analysis emphasizes the role of intermolecular orbital interactions among bonds or charge transfer and π - conjugation interaction in molecular systems. It is performed by considering all possible interactions between filled donor and empty acceptor natural bond orbital and estimating their energetic importance using second-order perturbation theory. The stabilization energy E_2 associated with electron delocalization between electron donor (i) and electron acceptor (j) is calculated according to the equation below.

$$E_2 = \Delta E_{(ij)} = \frac{q_i \left[F_{(ij)} \right]^2}{E_j - E_i} = q_i \frac{F_{ij}^2}{\Delta E} \qquad (13)$$

where q_i represent the orbital occupancy, E_j and E_i are diagonal elements(orbital energies) and $F_{(ij)}$ is the off-diagonal natural bond orbital Fock matrix elements. In this study, the natural localized molecular orbital that display the delocalization from Lewis orbital to a non-Lewis orbital corresponding to a stabilizing donor-acceptor interaction was predicted using B3LYP functional and LANL2DZ basis set. Nobel *et al*, (2017) reported that this provides additional evidence of the intermolecular delocalization effects.

DOI: 10.56892/bima.v8i1.636

From Table 1, it is observed that the values of the stabilization energy of the antibonding orbitals of the acceptor can interact with the lone pair (LP) of N_{23} and N_{24} of novel ADI derivatives as the donor orbital. The greatest stabilization energy values occur for $LP(2)N_{23} \rightarrow \pi^*(O_{19} - C_{26})$ and $LP(2)N_{24} \rightarrow \pi^*(O_{22} - C_{28})$ interactions with corresponding values of 70.48 Kcal/mol and 70.64 Kcal/mol respectively. Therefore we expect a strong donation interaction of the N_{23} and N_{24} atoms offering its Lone pair electrons to $\pi^*(O_{19} - C_{26})$ and $\pi^*(O_{22} - C_{28})$ respectively. This is also evident from the low value occupancy of N_{23} (1.32039e) and N_{24} (1.32117e) atoms. These electronic transitions are termed as $n \rightarrow \pi^*$ transitions since the energies are in the range 5.15 eV. This large delocalization energy indicates that the material exhibit higher first-order hyperpolarizability as can observed from Table 3 and the transition energy value in the visible region revealing the suitability of novel Anthracene diimide substituted halides for organic light emitting diodes application. Mahani *et al*, (2014) observed that many nitroso compounds usually demonstrate bright color due to their $n \rightarrow \pi^*$ electronic transitions. From Table 2, the greatest stabilization energies E_2 of non-bonding interactions of chlorine occurs for $LP(2)Cl_{29} \rightarrow \pi^*(C_1 - C_2)$, $LP(2)N_{24} \rightarrow \pi^*(C_{22} - C_{28})$, $LP(2)N_{23} \rightarrow \pi^*(C_{19} - C_{26})$ and $LP(2)Cl_{30} \rightarrow \pi^*(C_{14})$ with corresponding values of 59.79, 78.58, 80.53 and 115 Kcal/mol respectively. These increasing interaction energies are due to the strong intramolecular charge transfer leading to the stabilization of the novel ADI derivatives. The electronic transition are designated as $n \rightarrow \pi^*$ transitions with energies 8.68, 5.15, 5.15, and 3.79 eV respectively all being in the visible region of the spectra. As can be observed from Table 3, the greatest stabilization energy E_2 of non-bonding interactions of bromine halogen appears for $LP(2)Br_{29} \rightarrow \pi^*(C_1 - C_2)$ and $LP(2)Br_{29} \rightarrow \pi^*(C_{14} - C_{15})$ with corresponding value of about 24.18 Kcal/mol each. Bromine halogen is observed to have lower non-bonding stabilization energy, though with an electronic transition energy of about 21.69 eV and occupancy 1.87329e. These transitions again are in the visible region of the spectra and a possible OLED application. From Table 4, the greatest stabilization energy E_2 of delocalization are respectively 107.27 Kcal/mol and 111.11kcal/mol associated with the donor and $LP(3)O_{22} \rightarrow \pi^*(N_{24} - C_{28})$ acceptor interactions. This calculated results revealed that a very strong and intensive interaction between the p-type orbital containing the lone pair electrons of O_{19} and neighbors $\pi^*(N_{23} - C_{26})$ and $\pi^*(O_{24} - C_{28})$ antibonding orbital of the novel ADI derivatives. This interaction is responsible for the pronounced decrease of the lone pair orbital occupancy antibonding $\pi^*(N_{23} - C_{26})$ (1.539e) and $\pi^*(O_{24} - C_{28})$ (1.52338e).Again, the electronic transitions are designated as $n \rightarrow \pi^*$ with energies of 6.78 eV and 20.88 eV that are in the visible region of the spectra. As revealed from Table 1, 2, and 3 for the halogens, the second-order perturbation energies (also known as the stabilization energy) the most interacting natural bond orbital of the halogens between the lone pairs and nonbonding orbitals i.e. $LP(3)F_{29} \rightarrow \pi^*(C_{14} - C_{15})$, $LP(2)Br_{29} \rightarrow \pi^*(C_1 - C_2)$ and $LP(3)Cl_2 \rightarrow \pi^*(C_1 - C_2)$ are 19.7, 24.18 and

DOI: 10.56892/bima.v8i1.636

59.79 Kcal/mol respectively. These transitions are designated as usual by $n \rightarrow \pi^*$ transitions with energies 10.85, 8.68 and 21.69 eV respectively that are in the visible region of the spectra. It is reported that the stability of halogens generally increases down the group in the periodic table, though we observed a different trend here(Bisong *et al*, 2020). The entire trend observed can be attributed to the Electronegativity and negative inductive effect of the halogen atoms attached to the Anthracene backbone core.

Table 1: Second-order most Interaction energies of Donor and Acceptor orbitals of novel ADI-F_2 derivatives at B3LYP/LANL2DZ level of theory (gas phase)

Donor NBO	$E_j - E_i$ (a.u)	Bond Type	Occupancy	Acceptor	Bond Type	E_2 Kcal/mol
C_4- C_8	0.28	$\pi BD(2)$	1.51530	$C_2 - C_3$	$BD^*(2)$	23.77
$C_{11} - C_{13}$	0.27	$\pi BD(2)$	1.61871	$C_{14} - C_{15}$	$BD^*(2)$	24.76
C_1	0.16	$LP^*(1)$	0.92031	$C_2 - C_3$	$BD^*(2)$	60.51
C_9	0.14	$LP^*(1)$	0.99409	$C_4 - C_8$	$BD^*(2)$	68.85
N_{23}	0.19	$nLP(2)$	1.32039	$O_{19} - C_{26}$	$BD^*(2)$	70.48
N_{24}	0.19	$nLP(2)$	1.32117	$O_{22} - C_{28}$	$BD^*(2)$	70.64
F_{29}	0.40	$nLP(3)$	1.87771	$C_{14} - C_{15}$	$BD^*(2)$	19.72

Table 2: Second-order most Interaction energies of Donor and Acceptor orbitals of novelADI-Cl_2 derivative at B3LYP/LANL2DZ level of theory (gas phase).

Donor NBO	$E_j - E_i$ (a.u)	Bond Type	Occupancy	Acceptor	Bond Type	E_2 Kcal/mol
$C_5 - C_6$	0.25	$\pi BD(2)$	1.66206	C_1- C_2	$BD^*(2)$	24.06
$C_7 - C_{10}$	0.29	$\pi BD(2)$	1.53959	$C_9 - C_{15}$	$BD^*(2)$	24.04
$C_9 - C_{15}$	0.29	$\pi BD(2)$	1.58592	$C_9 - C_{10}$	$BD^*(1)$	25.00
C_3	0.11	$LP^*(1)$	0.97682	$C_1 - C_2$	$BD^*(2)$	104.47
C_{14}	0.21	$LP^*(1)$	1.01752	$C_9 - C_{15}$	$BD^*(2)$	50.43
O_{20}	0.59	$nLP(2)$	1.85554	$C_7 - C_{25}$	$BD^*(1)$	23.65
O_{21}	0.59	$nLP(2)$	1.85470	$C_8 - C_{27}$	$BD^*(1)$	23.65
O_{22}	0.63	$nLP(2)$	1.87793	$C_{15} - C_{28}$	$BD^*(1)$	21.29
N_{23}	0.19	$nLP(2)$	1.36896	$O_{19} - C_{26}$	$BD^*(2)$	80.53
N_{24}	0.19	$nLP(2)$	1.36108	O_{22}- C_{28}	$BD^*(2)$	78.58
Cl_{29}	0.32	$nLP(3)$	1.66299	$C_1 - C_2$	$BD^*(3)$	59.79

Bima Journal of Science and Technology, Vol. 8(1B) Apr, 2024 ISSN: 2536-6041

DOI: 10.56892/bima.v8i1.636

Table 3: Second-order most Interaction energies of Donor and Acceptor orbitals of novel ADI-Br_2 derivative at B3LYP/LANL2DZ level of theory (gas phase).

Donor NBO	$E_j - E_i$ (a.u)	Bond Type	Occupancy	Acceptor	Bond Type	E_2 Kcal/mol
$C_2 - C_3$	0.23	$\pi BD(2)$	1.62610	$C_1 - Br_{29}$	$BD^*(2)$	32.05
$C_4 - C_8$	0.29	$\pi BD(2)$	1.59502	$C_2 - C_3$	$BD^*(2)$	24.42
$C_5 - C_6$	0.22	$\pi BD(2)$	1.72906	$C_1 - Br_{29}$	$BD^*(2)$	31.07
$C_7 - C_{10}$	0.29	$\pi BD(2)$	1.59502	$C_9 - C_{15}$	$BD^*(2)$	24.41
$C_9 - C_{15}$	0.23	$\pi BD(2)$	1.62611	$C_{14} - Br_{30}$	$BD^*(2)$	32.05
$C_{11} - C_{13}$	0.22	$\pi BD(2)$	1.72900	$C_{14} - Br_{30}$	$BD^*(2)$	31.07
O_{19}	0.63	$nLP(2)$	1.85937	$C_2 - C_{26}$	$BD^*(1)$	20.63
O_{20}	0.60	$nLP(2)$	1.86288	$C_7 - C_{27}$	$BD^*(1)$	23.18
O_{21}	0.60	$nLP(2)$	1.86289	$C_8 - C_{25}$	$BD^*(1)$	23.18
O_{22}	0.63	$nLP(2)$	1.85937	$C_{15} - C_{28}$	$BD^*(1)$	20.63
N_{23}	0.19	$nLP(2)$	1.39300	$O_{19} - C_{26}$	$BD^*(2)$	99.34
N_{24}	0.17	$nLP(2)$	1.39295	$O_{22} - C_{28}$	$BD^*(2)$	99.35
Br_{29}	0.80	$nLP(2)$	1.87329	$C_1 - C_2$	$BD^*(1)$	24.18
Br_{30}	0.80	$nLP(2)$	1.87329	$C_{14} - C_{15}$	$BD^*(1)$	24.18

Table 4: Second-order most Interaction energies of Donor and Acceptor orbitals of novel ADI-I_2 derivative at B3LYP/LANL2DZ level of theory (gas phase).

Donor NBO	$E_j - E_i$ (a.u)	Bond Type	Occupancy	Acceptor	Bond Type	E_2 Kcal/mol
$C_2 - C_3$	0.21	$\pi BD(2)$	1.61676	$C_1 - I_{29}$	$BD^*(2)$	25.14
$C_4 - C_8$	0.28	$\pi BD(2)$	1.60567	$C_2 - C_3$	$BD^*(2)$	24.58
$C_7 - C_{10}$	0.28	$\pi BD(2)$	1.59642	$C_9 - C_{15}$	$BD^*(2)$	23.73
$C_9 - C_{15}$	0.19	$\pi BD(2)$	1.60711	$C_{14} - I_{30}$	$BD^*(2)$	32.07
$C_{11} - C_{13}$	0.19	$\pi BD(2)$	1.73796	$C_{14} - I_{30}$	$BD^*(2)$	27.20
$N_{23} - C_{26}$	0.31	$\pi BD(2)$	1.76513	$O_{20} - C_{25}$	$BD^*(2)$	37.90
$N_{24} - C_{28}$	1.39	$\pi BD(1)$	1.76157	$O_{21} - C_{27}$	$BD^*(2)$	38.66
O_{19}	0.77	$nLP(3)$	1.53084	$N_{23} - C_{26}$	$BD^*(2)$	107.27
O_{20}	0.61	$nLP(2)$	1.87375	$C_7 - C_{25}$	$BD^*(1)$	22.16
O_{21}	0.61	$nLP(2)$	1.87292	$C_8 - C_{27}$	$BD^*(1)$	22.21
O_{22}	0.25	$nLP(3)$	1,52338	$N_{24} - C_{28}$	$BD^*(2)$	111.11

DOI: 10.56892/bima.v8i1.636

UV-Vis Spectroscopic Studies

The electronic properties of ADI-Rb_2F_2, ADI-Rb_2Cl_2, ADI-Rb_2Br_2 and ADI-Rb_2I_2 have been calculated at TD-DFT/B3PW91 level in conjunction with LANL2DZ basis sets in the gas phase. We have calculated the excited states by specifying the excitation energies, maximum wavelength λ_{max} , and the oscillator strength (f), as shown in Table 5. The oscillator strength is the measure of how strongly a particular electronic transition is allowed in absorption (Misha and Prakash, 2020). The theoretical calculated UV-vis spectrum of these novels Anthracene diimide derivatives are shown in Figure 2. The UV-vis spectroscopies were plotted with the help of GaussSum 3.0 version (O'Boyle *et al*, 2008). The TD-DFT calculations revealed a number of different electronic transitions for each of novel Anthracene diimide substituted -Rb_2F_2, -Rb_2Cl_2, -Rb_2Br_2, and –Rb_2I_2 derivatives. From Figure 2, three major UV-vis absorption transitions of ADI-Rb_2F_2 have maximum wavelength λ_{max} values of 543.85, 627.75, and 902.9 nm respectively. The results suggest that the introduction of -Rb_2F_2 group can enhance optoelectronic properties of Anthracene diimide derivative. The transition excitation energies are 1.3762, 1.9483, 2.2798 eV and oscillator strength (f) range from 0.0650-0.0839 respectively. The ultraviolet analysis of ADI-Rb_2Cl_2 predicts only one major electronic transition that is responsible for the absorption band. The maximum wavelength λ_{max} peak occurs at 624.4 nm with oscillator strength (f) 0.0988 and vertical excitation energy 1.9890 eV. The major electronic transition of ADI-Rb_2Br_2 was observed to have a maximum wavelength λ_{max} 648.40 nm and oscillator strength (f) 0.0874 with vertical excitation energy of 1.9122 eV. On the other hand, low electronic transition was observed to have maximum wavelength, oscillator strength and vertical excitation energy of 713.89 nm, 0.0109 and 1.7389 eV respectively. Finally, ADI-Rb_2I_2 has five predicted major electronic transitions maximum wavelength peaks 641.04, 695.93, 770.94 and 1239.27, 2000 nm respectively. The maximum wavelength λ_{max} peak occurs at 2000 nm with oscillator strength (f) 0.0488. We assume that it should be the most sensitive Anthracene diimide derivative. Values of the vertical excitation energies are in the range 1.9341-0.6426 eV. It is clear that 0scillator strength has increased (i.e. 0.0019, 0.0140, 0.0162, 0.0103 and 0.0488) due to the introduction of –Rb_2I_2, group to Anthracene diimide organic semiconductor. These compounds can be utilized for practical applications. It is observed from these theoretical calculated results that the maximum wavelength of the novel Anthracene diimide substituted rubidium halides are in the order of $ADI-Rb_2I_2\rangle\, ADI-Rb_2F_2\rangle\, ADI-Rb_2Br_2\rangle\, ADI-Rb_2Cl_2\rangle$, maximum vertical excitation energies are in the order of $ADI-Rb_2F_2\rangle\, ADI-Rb_2Cl_2\rangle\, ADI-Rb_2I_2\rangle\, ADI-Rb_2Br_2\rangle$ and the oscillator strength are of the order $ADI-Rb_2Cl_2\rangle 0.0988\, ADI-Rb_2Br_2\rangle 0.0871\, ADI-Rb_2F_2\rangle 0.0677\, ADI-Rb_2I_2\rangle 0.0488$ respectively.

In the case of Anthracene diimide halides (ADI-F_2, ADI-Cl_2, ADI-Br_2 and ADI-I_2) the UV-Vis absorption spectrum displays a broad absorption peaks at 570.0, 798.33, and 1239.5 nm for **ADI-F_2,** at 585.44, 744.46, and 1165.11 nm for ADI-Cl_2, at 591.43, 783.77, and 1145.01 nm for ADI-Br_2, at 676.17, 899.06, and 1162.94 nm for ADI-I_2 respectively. The different UV-Vis absorption spectrum intensities of these molecules are in the maximum range of 585.44 - 1239.5 nm and corresponding to $\pi-\pi^*$ transition of the ADI

DOI: 10.56892/bima.v8i1.636

core with TD-DFT calculations. Usta *et al*, (2012) have reported that the absorption spectra of ADI derivatives exhibit maxima at 418-436 nm of the ADI core. The oscillator strength of the ADI-halide is much higher than the rubidium halides. It is observed that the incorporation of electron-withdrawing halides and rubidium-halide units into layered organic molecules would present interesting inter and intramolecular interactions as well as new optoelectronic properties greatly enriching organic functional materials.

HOMO-LUMO and Frontier Molecular Orbitals

To gain more insight into the electronic properties of halides and rubidium-halides substituted Anthracene diimide, the frontier molecular orbital, and HOMO and LUMO levels were obtained by TD-DFT calculations at B3PW91/Lanl2dz level of theory. The HOMO and LUMO are the main orbitals responsible for chemical stability while the frontier molecular orbital energy that characterizes chemical reactivity and kinetic stability of organic molecules. Molecules with small frontier orbital energies will possess high chemical reactivity or high conductivity and low kinetic stability. Table 6 depicts the calculated energies, HOMO, LUMO and the band gap energies of the halides/rubidium-halides substituted Anthracene diimide at B3PW91 level.

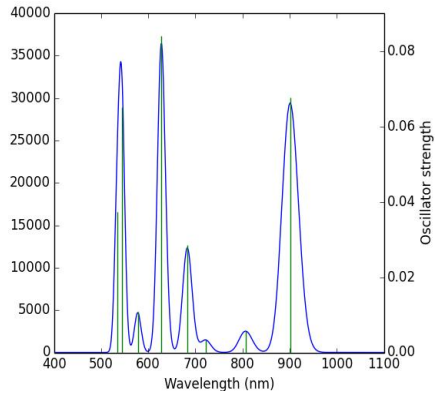

(a) ADI-Rb_2F_2

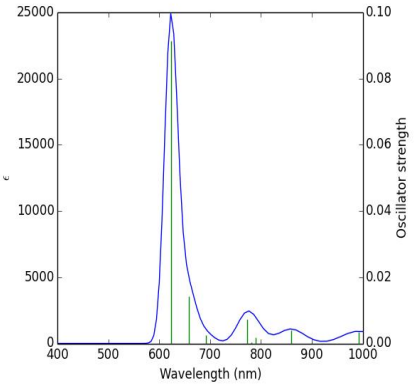

(b) ADI-Rb_2Cl_2

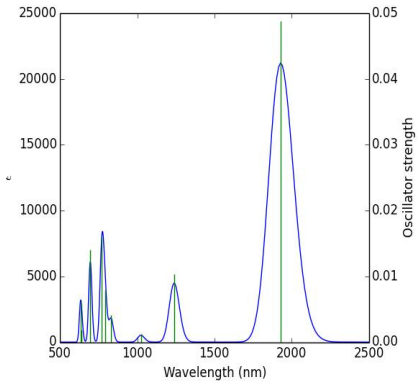

(c) ADI-Rb_2I_2

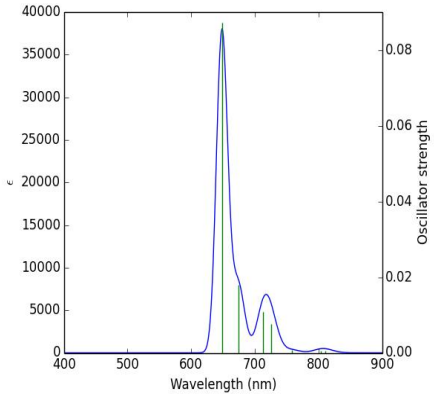

(d) ADI-Rb_2Br_2

Figure 2**:** UV-vis Spectra of Rubidium halides substituted Anthracene diimide of ADI-Rb_2F_2,ADI-Rb_2Cl_2 , ADI-Rb_2I_2, and ADI-Rb_2Br_2 at B3W91/LANL2DZ Level.

As depicted from Table 6, the calculated energy of pure Anthracene diimide is about -1099.17 eV. The calculated energies for Anthracene halides and Anthracene rubidium-

DOI: 10.56892/bima.v8i1.636

halides i.e. ADI-F_2, ADI-Cl_2, ADI-Br_2, ADI-I_2, ADI-Rb_2F_2, ADI-Rb_2Cl_2, ADI-Rb_2Br_2, and ADI-Rb_2I_2 are -1297.56, -1127.59, -1122.92, -1118.71, -1341.98, -1172.37, -1168.94 and -1165.16 eV respectively. It is observed that all the calculated energies are negative and the negativity decreases as we go across from the least organic molecule to the greatest. ADI-F_2 and ADI-Rb_2F_2 calculated values are more negative relative to the value of pure Anthracene diimide, thus they are more stable. This account for the fact that fluorine is more electronegative atom as compared to other halides and substitution of fluorine makes organic molecules polar bonds. The structural stability of the organic molecules gradually increases with the increase in the number of atoms. Furthermore, as the number of atoms increases, it becomes more stable. The HOMO/LUMO for Anthracene diimide, ADI is about -7.67/-6.59 eV while the HOMO/LUMO of ADI-F_2, ADI-Cl_2, ADI-Br_2, ADI-I_2, ADI-Rb_2F_2, ADI-Rb_2Cl_2 , ADI-Rb_2Br_2, and ADI-Rb_2I_2 are -7.92/-6.86, -7.36/-6.29, -6.78/-5.79, -6.22/-5.66, -5.51/-4.91, -4.71/-4.15, -3.02/-4.04 and -2.39/-3.86 eV respectively. E_{HOMO} is often associated with the electron-donating ability while the E_{LUMO} designate the ability to accept electron. According to these results obtained from TD-DFT calculation using restricted B3PW91/Lanl2dz level, the values of E_{HOMO} and E_{LUMO} shows a decreasing trend of the properties of Anthracene diimide substituted halides and rubidium-halides respectively. This is consistent with reports from literature revealing that attaching F_2 and Br_2 atoms to π-conjugated system lower the LUMO energy (Yin *et al*, 2016). Similarly, the calculated LUMO energies obtained here for ADI-Br_2 (-5.79 eV)and ADI-Rb_2Br_2 (-4.04 eV) are in the range of those calculated for air-stable n-channel ADI semiconductors (Usta *et al*, 2012). The HOMO and LUMO orbital isosurfaces of the Anthracene derivatives are depicted in Figure 3; their energies and energy gap ΔE_g are presented and discussed (Table 6). It is seen from Figure 3 that with the HOMOs, the delocalization occur mainly on the imides rings in the π -conjugated backbone of ADI with different energy levels. In contrast, the LUMOs show an efficient delocalization of the Anthracene backbone and diimide bonds that result in low-lying LUMO energy levels. Also the LUMOs have large contribution from the electron-withdrawing moieties. As can be seen from Table 6, the results depict that the energy band gap ΔE_g contracts from 1.08 to 0.43 eV calculated using B3PW91 functional and Lanl2dz basis set upon addition of halides and rubidium halides substituted Anthracene diimide. The decrease in ΔE_g values explains the eventual charge transfer interaction taking place within the ADI-F_2, ADI-Cl_2, ADI-Br_2, ADI-I_2, ADI-Rb_2F_2, ADI-Rb_2Cl_2, ADI-Rb_2Br_2, and ADI-Rb_2I_2 respectively. The energy band gap ΔE_g , is the difference between the HOMO and LUMO, decreases with an increase in conjugation when incorporated with additional atoms or units into the π-conjugated backbone where discrete π and π^* orbitals begin to stack upon each other. Studies revealed that the energy band gap E_g obtained from optical data lies in the range 1.0-1.3 eV which is consistent with our results as well as comparable to our unsubstituted Anthracene diimide π -conjugated small molecule (Sam-Shajing and Larry, 2017). Other factors responsible for lower band gap energy E_g include planarity caused by the rigidification of the π -conjugation and the less steric interactions between neighboring monomer groups as there is no hydrogen atom attached to the nitrogen. These bands are also referred to as valence band and conduction band. These substituent groups regulate the electronic energy levels and help improve the absorption spectra of the conjugated organic materials.

DOI: 10.56892/bima.v8i1.636

Table 5:UV-Vis Spectra of ADI-Rb_2F_2, ADI-Rb_2Cl_2, ADI-Rb_2Br_2 and ADI-Rb_2I_2 of Anthracene derivatives in the gas phase.

Compound	Excited Energies (eV)	Absorbed Wavelength(nm)	Oscillator Strength(f)
ADI-Rb_2F_2	0.2648	4682.57	0.0000
	0.4057	3055.81	0.0072
	0.8865	1398.58	0.0009
	1.3762	902.9	0.0677
	1.5375	806.41	0.0058
	1.7186	721.41	0.0034
	1.8159	682.78	0.0284
	1.9751	627.75	0.0839
	2.1465	577.62	0.0108
	2.2798	543.85	0.0650
	2.3212	534.14	0.0374
ADI-Rb_2Cl_2	0.2027	6115.81	00008
	0.4950	2504.87	0.0696
	1.000	1239.83	0.0037
	1.2502	991.73	0.0034
	1.4427	859.96	0.0040
	1.5689	790.24	0.0017
	1.5863	781.59	0.0004
	1.6053	772.33	0.0074
	1.7934	691.34	0.0026
	1.8834	658.30	0.0142
	1.9890	623.35	0.0993
ADI-Rb_2Br_2	0.1892	6551.96	0.0007
	0.3593	3451.16	0.0432
	0.9377	1322.23	0.0019
	1.1823	1048.67	0.0036
	1.5291	810.82	0.0006
	1.5417	804.20	0.0006
	1.6354	758.13	0.0008
	1.7080	725.89	0.0077
	1.7389	713.00	0.0109
	1.8388	874.27	0.0180
	1.9122	648.40	0.0871
ADI-Rb_2I_2	0.1176	10539.5	0.0044
	0.6426	1929.31	0.0488
	1.0005	1239.27	0.0103
	1.2104	1024.35	0.0012
	1.4931	830.39	0.0041
	1.5688	790.30	0.0079
	1.6082	770.94	0.0162
	1.7384	713.22	0.0001
	1.7815	695.93	0.0140
	1.9341	641.04	0.0019
	1.9602	632.52	0.0061

DOI: 10.56892/bima.v8i1.636

HOMO **LUMO**

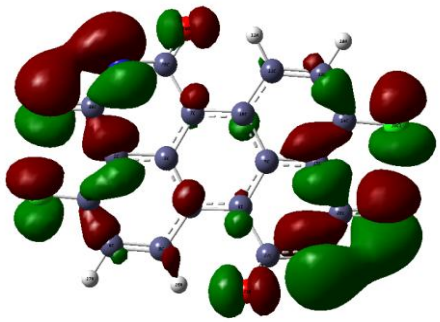

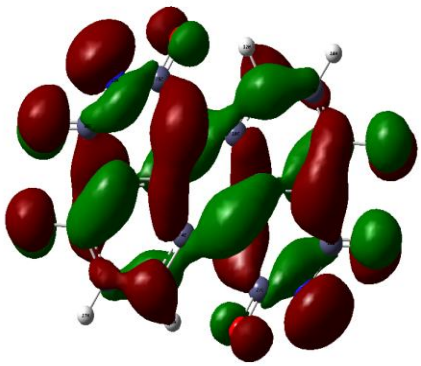

a.ADI-Cl_2 b. ADI-Cl_2

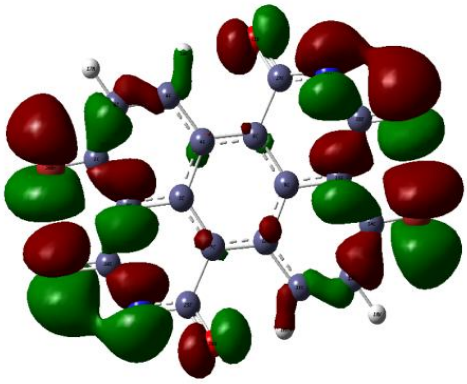

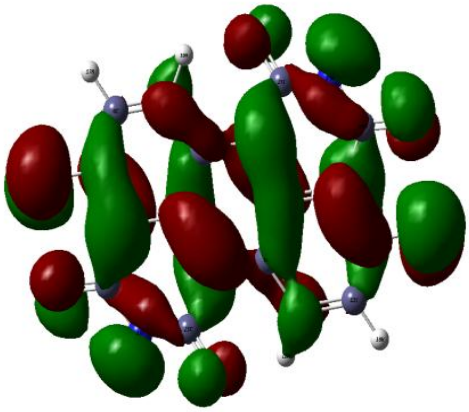

c.ADI-Br_2 d. ADI-Br_2

Figure 3: HOMO and LUMO orbitals Anthracene diimide derivatives calculated at B3PW91/Lanl2dz level of theory

DOI: 10.56892/bima.v8i1.636

Table 6: E_{HOMO}, E_{LUMO}, ΔE_g (eV) of Anthracene diimide obtained using TD-DFT levels at Lanl2dz basis sets.

Compound	Calculated Energy(eV)	E_{HOMO}(eV)	E_{LUMO} (eV)	ΔE_g (eV)
Pure-ADI	-1099.17	-7.67	-6.59	1.08
ADI-F_2	-1297.56	-7.92	-6.86	1.06
ADI-Cl_2	-1127.58	-7.36	-6.29	1.07
ADI-Br_2	-1122.92	-6.78	-5.79	0.99
ADI-I_2	-1118.71	-6.12	-5.66	0.76
ADI-Rb_2F_2	-1341.98	-5.51	-4.91	0.60
ADI-Rb_2Cl_2	-1172.36	-4.71	-4.15	0.56
ADI-Rb_2Br_2	-1168.94	-3.02	-4.04	0.50
ADI-Rb_2I_2	-1165.16	-2.39	-3.86	0.43

Nonlinear Optical Properties (NLO)

The estimated nonlinear optical property values of dipole moment (μ), linear polarizability (α), and first-order hyperpolarizability(β) for static and frequency-dependence using restricted HF and B3LYP functionals with Lanl2dz basis sets were computed for novel Anthracene diimide derivatives in the gas phase are listed in Table 7 and 9. These nonlinear components indicate the non-uniform charge distribution along the three directions. Nonlinear optical properties change with the change in theoretical method. Maroulis and Haskopoulos (2010), have shown the functional dependence of dipole moment, polarizability and first-order hyperpolarizability.

Table 7 shows the dipole moment μ of novel Anthracene diimide derivatives ADI-F_2, ADI-Cl_2, ADI-Br_2, ADI-I_2, ADI-Rb_2F_2, ADI-Rb_2Cl_2, ADI-Rb_2Br_2, and ADI-Rb_2I_2 obtained at restricted HF and B3LYP level of theory in conjunction with Lanl2dz basis set using equation ten(10) above. From the Table the total dipole moment estimated with B3LYP functional for the halide and rubidium halide substituted Anthracene diimide derivatives ADI-F_2, ADI-Cl_2, ADI-Br_2, ADI-I_2, ADI-Rb_2F_2, ADI-Rb_2Cl_2, ADI-Rb_2Br_2, and ADI-Rb_2I_2 are 0.0097, 0.7096, 0.0011, 0.4940, 3.5721, 4.1830, 4.400, and 4.8091 D respectively. Similarly, the total dipole moment estimated with restricted HF functional for the halide and rubidium halide substituted Anthracene diimide derivatives ADI-F_2, ADI-Cl_2, ADI-Br_2, ADI-I_2, ADI-Rb_2F_2, ADI-Rb_2Cl_2, ADI-Rb_2Br_2, and ADI-Rb_2I_2 are 0.0148, 0.9933, 0.0014, 0.9319, 4.0670, 6.0781, 7.4993, 7.1176 D respectively. This variation in the total dipole moment at both levels of theory is attributed to an overall imbalance of the charge distribution from one side of the organic molecule to the other. The dipole moment components indicate the non-uniform charge distribution along the three directions, x, y, and z. These total dipole moment values are far less than the dipole moment of μrea (i. e. μrea μ = 1.3732 D) for halides substituted Anthracene diimide at the both levels of theory and remarkably higher than μrea for rubidium halide substituted Anthracene diimide at both levels (Mutha *et al*, 2014; Arshad *et al*, 2017). The values of these novel Anthracene diimide derivatives may significantly contribute towards its reactivity.

From Table 8, the static polarizability (i.e. $\alpha(0)$ or $\alpha(0,0)$) of ADI-F_2, ADI-Cl_2, ADI-Br_2, ADI-I_2, ADI-Rb_2F_2, ADI-Rb_2Cl_2, ADI-Rb_2Br_2, and ADI-Rb_2I_2 estimated at RHF/Lanl2dz level are found to be 45.5 x 10^{-24}, 44.1 x 10^{-24}, 46.5 x 10^{-24}, 54.2 x 10^{-24}, 67.6 x 10^{-24}, 75.7 x 10^{-24}, 47.1 x 10^{-24}, 82.2 x 10^{-24} esu respectively. Similarly the static polarizability

DOI: 10.56892/bima.v8i1.636

(i.e. $\alpha(0)$ or $\alpha(0,0)$) of ADI-F_2, ADI-Cl_2, ADI-Br_2, ADI-I_2, ADI-Rb_2F_2, ADI-Rb_2Cl_2, ADI-Rb_2Br_2, and ADI-Rb_2I_2 estimated at RB3LYP/Lanl2dz level are 47.6 x 10^{-24}, 50.2 x 10^{-24}, 52.7 x 10^{-24}, 62.2 x 10^{-24}, 86.6 x 10^{-24}, 85.7 x 10^{-24}, 92.7 x 10^{-24}, 107.8 x 10^{-24} esu respectively.It is observed from these results of the static polarizability (i.e. $\alpha(0)$ or $\alpha(0,0)$) calculated with RB3LYP functional are positive and higher than those calculated with RHF functional. Nonlinear optical properties are sensitive to functionals used in the calculation. In the case of frequency-dependent polarizability (i.e. $\alpha(\omega = 0.02389)a.u$) the novel Anthracene diimide derivatives ADI-F_2, ADI-Cl_2, ADI-Br_2, ADI-I_2, ADI-Rb_2F_2, ADI-Rb_2Cl_2, ADI-Rb_2Br_2, and ADI-Rb_2I_2 estimated at RHF/Lanl2dz level are 48.6 x 10^{-24}, 45.3 x 10^{-24}, 47.8 x 10^{-24}, 56.2 x 10^{-24}, 13.9 x 10^{-24}, 45.3 x 10^{-24}, 58.7 x 10^{-24},53.6 x 10^{-24} esu while the predicted values for RB3LYP/Lanl2dz level are 47.9 x 10^{-24}, 56.3 x 10^{-24}, 61.3 x 10^{-24}, 54.4 x 10^{-24}, 51.3 x 10^{-24}, 40.6 x 10^{-24}, 48.2 x 10^{-24}, and 46.2 x 10^{-24} esu respectively. The frequency-dependent polarizability values for RHF functional are far greater and positive than the values of RB3LYP functional. The variations in the values of the polarizability are due to the sensitivity of this nonlinear optical property to the functional. These results suggest that the introduction of –F_2, -Cl_2,-Br_2, -I_2, -Rb_2F_2, -Rb_2Cl_2, -Rb_2Br_2, and –Rb_2I_2 atoms and groups can be helpful to enhance the nonlinear response.

In this work, we use $\beta(0,0,0)$ and $\beta(-\omega,\omega,0)$ static and dynamic first-order hyperpolarizability. The expression for calculating the magnitude of dynamic first-order hyperpolarizability from Gaussian 09 output is given by the equation (12). This nonlinear optical property gives information about the organic π -conjugated small molecule Anthracene diimide derivative capacity to generate second-order nonlinear effects. Table 8 shows the static and frequency-dependent first-order hyperpolarizability (β) of novel Anthracene diimide derivatives ADI-F_2, ADI-Cl_2, ADI-Br_2, ADI-I_2, ADI-Rb_2F_2, ADI-Rb_2Cl_2, ADI-Rb_2Br_2, and ADI-Rb_2I_2 values predicted for RHF and B3LYP functionals. From the Table, the static first-order hyperpolarizability (β), calculated using RHF/Lanl2dz functional for ADI-F_2, ADI-Cl_2, ADI-Br_2, ADI-I_2, ADI-Rb_2F_2, ADI-Rb_2Cl_2, ADI-Rb_2Br_2, and ADI-Rb_2I_2 are found to be 0.36, 5.5, 0.007, 14.3, 448.5, 1871.5, 31.4, and 7572.4 x 10^{-30} (esu) respectively. These results revealed that the lowest value is 0.007 x 10^{-30} (esu) for ADI-Br_2 among all the Anthracene diimide derivatives which suggest that it might be due to less conjugation of the Bromine to the Anthracene backbone. Similarly, the static first-order hyperpolarizability (β), calculated using B3LYP/Lanl2dz functional for ADI-F_2, ADI-Cl_2, ADI-Br_2, ADI-I_2, ADI-Rb_2F_2, ADI-Rb_2Cl_2, ADI-Rb_2Br_2, and ADI-Rb_2I_2 are found to be 0.016, 5.1, 0.008, 6.8, 88.4, 10.4, 8.6, and 22.2 x 10^{-30} (esu) respectively. ADI-Rb_2F_2 has the highest first-order hyperpolarizability value among all the other Anthracene derivatives due to the strong electron acceptor F_2 at the end-side of the Anthracene backbone core that enhance the nonlinear optical response. These static first-order hyperpolarizability calculated at RHF and B3LYP are approximately 1.9, 28, 73, 161, 2309 (with RHF) and 0.08, 26, 35, 44, 53, 114, and 454 (with B3LYP) times greater than urea (i.e. β of urea = 0.1947 x 10^{-30} esu). These results indicate that Anthracene diimide substituted halides and rubidium halides are nonlinear. For the case of frequency-dependent first-order hyperpolarizability $\beta(-\omega,\omega,0)$ the Anthracene diimide derivatives ADI-F_2, ADI-Cl_2, ADI-Br_2, ADI-I_2, ADI-Rb_2F_2, ADI-Rb_2Cl_2, ADI-Rb_2Br_2, and ADI-Rb_2I_2 computed at RHF/Lanl2dz and B3LYP/Lanl2dz are found to be 0.78, 7.46, 13.8, 464.7, 204.1, 22290, 171.2 x 10^{-30} esu and 1.2, 69.5, 1.52, 20.9,

DOI: 10.56892/bima.v8i1.636

4447.8, 223.2, 62.9, 1067.2 x 10^{-30} esu respectively. Within each method the calculated first-order hyperpolarizability vary due to the fact that some of the halogens are more electronegative than others and its contribution is less. The difference between the values is attributed to the computational method. As observed from the Table, the frequency-dependent first-order hyperpolarizability are large and non-zero and suggest that Anthracene diimide derivatives ADI-F_2, ADI-Cl_2, ADI-Br_2, ADI-I_2, ADI-Rb_2F_2, ADI-Rb_2Cl_2, ADI-Rb_2Br_2, and ADI-Rb_2I_2 might acquire microscopic second and third order nonlinear response. Furthermore, the frequency-dependent first-order hyperpolarizability of the Anthracene diimide derivatives ADI-F_2, ADI-Cl_2, ADI-Br_2, ADI-I_2, ADI-Rb_2F_2, ADI-Rb_2Cl_2, ADI-Rb_2Br_2, and ADI-Rb_2I_2 are all greater than the value of urea (β = 0.1947 x 10^{-30} esu). The values of the dipole moment and first-order hyperpolarizability are closely related to the electron delocalization strength as reflected in the E_2 behavior. A larger electronic delocalization parameter leads to a higher first-order hyperpolarizability value. These high values are produced due to dipole and molecular alignment and also from non-covalent interactions.

Table 7**:** The Dipole moment, of novel Anthracene diimide derivatives

		μ_x	μ_y	μ_z	$\langle\mu\rangle$
ADI-F_2	B3LYP	-0.0021	0.0025	-0.0096	0.0097
	HF	-0.0058	0.0045	-0.0128	0.0128
ADI-Cl_2	B3LYP	-0.6901	-0.1626	-0.0287	0.7096
	HF	-0.9923	0.0310	-0.0318	0.9933
ADI-Br_2	B3LYP	-0.0006	-0.0004	-0.0009	0.0011
	HF	0.0002	-0.0002	-0.0014	0.0014
ADI-I_2	B3LYP	-0.4742	-0.1340	-0.0353	0.4940
	HF	-0.9167	0.1652	-0.0311	0.9319
ADI-Rb_2F_2	B3LYP	3.5550	-0.3483	-0.0183	3.5721
	HF	4.0094	-0.6813	0.0268	4.0670
ADI-Rb_2Cl_2	B3LYP	3.0878	2.8125	-0.2313	4.1830
	HF	2.9958	5.2826	-0.2493	6.0781
ADI-Rb_2Br_2	B3LYP	1.0428	4.2802	-0.1518	4.4000
	HF	2.1573	7.1823	-0.0043	7.4993
ADI-Rb_2I_2	B3LYP	-2.8908	3.8428	-0.0865	4.8091
	HF	-4.3050	5.6662	0.1480	7.1176

DOI: 10.56892/bima.v8i1.636

Table 8: Total Static, Dynamic Polarizability and Hyperpolarizability of Anthracene diimide derivatives

Static($\omega = 0$)				Dynamic ω =0.0238	
compound	level	$\langle\alpha\rangle_{tot}$ x 10^{-24} (esu)	$\beta_{tot}(-\omega,\omega,0$ x 10^{-30} esu	$\langle\alpha\rangle_{tot}$ x10^{-24} (esu	$\beta_{tot}(-\omega,\omega,0)$ x 10^{-30} esu
ADI-F_2	B3LYP	47.6	0.016	47.9	1.2
	HF	45.5	0.30	48.6	0.78
ADI-Cl_2	B3LYP	50.5	5.1	56.3	69.5
	HF	44.1	5.5	45.3	7.5
ADI-Br_2	B3LYP	52.7	0.008	61.3	1.5
	HF	46.5	0.007	47.8	0.005
ADI-I_2	B3LYP	62.2	6.8	54.4	20.1
	HF	54.2	14.3	56.2	13.8
ADI-Rb_2F_2	B3LYP	86.6	88.4	51.3	4447.8
	HF	67.6	448.8	13.9	464.7
ADI-Rb_2Cl_2	B3LYP	85.7	10.4	40.6	223.2
	HF	75.7	1871.5	45.3	204.1
ADI-Rb_2Br_2	B3LYP	92.7	8.6	48.2	62.9
	HF	47.1	31.4	58.7	22290.3
ADI-Rb_2I_2	B3LYP	107.8	22.2	46.2	1067.2
	HF	82.2	7572.4	53.6	171.2

CONCLUSION

The present study investigated the electronic and nonlinear optical properties of ADI-F_2, ADI-Cl_2, ADI-Br_2, ADI-I_2, ADI-Rb_2F_2, ADI-Rb_2Cl_2, ADI-Rb_2Br_2, and ADI-Rb_2I_2 respectively using theoretical calculations based on the density functional method via B3PW91, B3LYP and HF functionals with Lanl2dz basis sets both in static and dynamic cases. The difference between these two groups of compound stem from the type of substituent though their position on the Anthracene backbone does not change. However, the change of substituent on the electric properties on the conjugated organic semiconductor is explored. Our calculations were made for the isolated conjugated organic molecules in the gas phase.

Our calculations indicated that the E_{HOMO} and E_{LUMO} energies of halides and rubidium halides substituent in the side position of the Anthracene diimide backbone varies and decreases. Most systems have different HOMO and LUMO compositions. Also, the HOMO-LUMO energy band gap E_g , calculations varies in the range 1.08 to 0.43 eV calculated using B3PW91 functional in conjunction with Lanl2dz basis sets. These substituent groups regulate the electronic energy levels and help improve the absorption spectra of organic π -conjugated small molecules. The nonlinear optical properties were calculated with the help of density functional theory. The results of the calculated total static polarizability of Anthracene diimide derivatives are all positive at both levels of the functional with B3LYP having higher calculated values than at RHF functional. The reverse is the case for the frequency-dependent polarizability calculated at $\alpha(\omega = 0.023890)$ a.u. The total static and total dynamic first order hyperpolarizability are non-zero and positive with values far greater than the standard compound urea, consequently they might be good candidates for advanced nonlinear materials.

REFERENCES

Arshad M. N. Al-Anood A. A. Abdulluh M. S. Muhammad K. Abdulhadi S. B. Khalid A.

DOI: 10.56892/bima.v8i1.636

A. Atanalpa A. C. B. (2017). Synthesis, Crystal Structure, Spectroscopic and nonlinear Optical Properties of Chalcone Derivatives: A Combined Experimental and Theoretical Study. Journal of Molecular Structure. 141, pp 142-156. Elsevier.

Atafa A. A. Samia K. Amin B. (2018). Spectral Calculations with Density Functional Theory. Recent Progress of Theory and Applications. IntechOpen, pp 101-127.

Atkins P. W. and Friedman R. S. (2005). Molecular Quantum Mechanics, 4th Edition, Oxford University Press.

Bisong E. A. Louis H. Unimuke T.O. Odey J. O. Ubana E.I. Edim M. M. Tizhe F. T. Agwupuye J. A. (2020). Vibrational, Electronic, Spectroscopic properties and NBO analysis of p- xylene, 3,6-difluoro-p-xylene, 3,6-dichloro-p-xylene and 3,6-dibromo- p- xylene: DFT Study. Heliyon 6.e05783, pp 1-14.

Bulik I. W. Zalesny R. Wojciech B. Josep M. L. Kirtman B. Scuseria G. E. Avramopoulos A. Reis H. Papadopoulos M. G. (2013).Performance of DFT in Computing Nonresonant Vibrational (Hyper) polarizability. Journal of Computational Chemistry, 34, pp 1775-1784

Casida M. E. (1995). Time - Dependent Density Functional Response Theory for Molecules. Recent Advances in Density Functional Method. pp 155-192.

Casida M. E. (2009). Time Dependent Density Functional Theory for Molecules and Molecular Solids. Journal of Molecular Structure: TheoChem, 914, pp 3-18. Elsevier.

Coropceanu V. Jerome C. Demetrio A. S. F. Yoanu O., Robert S., Bredas J.L.(2007). Charge Transport in Organic Semiconductor. Chemical Reviews, Vol. 107, No. 4, pp926-952.

Ding F. Benjamin E. Van K. Bruce E. E. Xiaosong L. (2013). An Efficient Method for Calculating Dynamical Hyperpolarizability Using real-time time-Dependent Density Functional Theory. Journal of Chemical Physics, 138(6), 064104.

Frisch M. J.; Trucks, G. W.; Schlegel, H. B.; Scuseria, G. E.; Robb, M. A.; Cheeseman, J. R.; Scalmani, G.; Barone, V.; Mennucci, B.; Petersson, G. A.; Nakatsuji, H.; Caricato, M.; Li, X.; Hratchian, H. P.; Izmaylov, A. F.; Bloino, J.; Zheng, G.; Sonnenberg, J. L.; Hada, M.; Ehara, M.; Toyota, K.; Fukuda, R.; Hasegawa, J.; Ishida, M.; Nakajima, T.; Honda, Y.; Kitao, O.; Nakai, H.; Vreven, T.; J. A. Montgomery, J.; Peralta, J. E.; Ogliaro, F.; Bearpark, M.; Heyd, J. J.; Brothers, E.; Kudin, K. N.; Staroverov, V. N.; Kobayashi, R.; Normand, J.; Raghavachari, K.; Rendell, A.; Burant, J. C.; Iyengar, S. S.; Tomasi, J.; Cossi, M.; Rega, N.; Millam, J. M.; Klene, M.; Knox, J. E.; Cross, J. B.; Bakken, V.; Adamo, C.; Jaramillo, J.; Gomperts, R.; Stratmann, R. E.; Yazyev, O.; Austin, A. J.; Cammi, R.; Pomelli, C.; Ochterski, J. W.; Martin, R. L.; Morokuma, K.; Zakrzewski, V. G.; Voth, G. A.; Salvador, P.; Dannenberg, J. J.; Dapprich, S.; Daniels, A. D.; Farkas, O.; Foresman, J. B.; Ortiz, J. V.; Cioslowski, J.;

DOI: 10.56892/bima.v8i1.636

Fox, D. J. In *Gaussian 09*; Revision A. 02; Gaussian, Inc.: Wallingford CT, **2009**

Kohn W. and Hohenberg P. (1964). Inhomogeneous electron gas. *Physical Review B*, 136, 864.

Kohn W. and Sham L. J. (1965). Self-Consistent Equations including Exchange and Correlation Effects. *Physical Review A, Vol.140, no.4A pp1133-1138*.

Kukhta A. V. Kukhta I. V. Kukhta N.A. Neyra O.L. Meza E.(2008). DFT Study of the Electronic Structure of Anthracene Derivatives in their anion and cation forms. Journal of Physics B: Atomic Molecular Optical Physics, 41, pp 1-7.

Lazaar K. Gueddida S. Foerster D. Said M.(2020).A Theoretical Investigation of the Effect of Fluorination and bromination on the Optoelectronic Properties of Tetrathienophenazine derivatives. *Computational Material Science*, 177, 109578.

Li C. Wei J. Xiaozhang Z. and Zhoohui W.(2014). Synthesis and properties of Diazapentancene. *Asian Journal of Organic Chemistry*, Vol. 3, pp 114-117. Communication.

Liu A. Mengfan G. Yan M. Xuefeng R. Liguo G. Yanqiang L. Tingli M.(2021). Theoretical Study of the influence of Doped Oxygen group Elements on the Properties of Organic Semiconductor. *Nanoscale Advances*, pp 1-7. Royal Society of Chemistry.

Mahani N. M. Saeidi F. Mirparizi E. (2014). Study of the Molecular Properties and Natural Bond Orbital Analysis of some Acyloxy Nitroso Compounds by Density Functional Theory Method. *Physical Chemistry an Indian Journal*, Vol.9 (8), pp 261-266.

Maroulis G. and Haskopoulos A. (2010). Interaction Electric Hyperpolarizability effects in Weakly Bound H_2O ------- R_g (R_g = He, Ne, Ar, Kr, and Xe) Complexes. Journal of Physical Chemistry A. Vol.114, Number 33, pp 8730-8741.

Marques M. A. L. and Gross E. K. U. (2004). Time-Dependent Density Functional Theory. *Annual Review Physical Chemistry*, 55, pp 427-455.

Mishra A. K. and Prakash S. T.(2020).DFT Calculations of Spectral, NLO, Reactivity, Natural bond orbital Properties and Docking Study of Vincosamide-N-Oxide active against Lung cancer cell lines H1299. Applied Sciences 2, 1021.

Mohebbi A, R. Munoz C. Wudl F. (2011). Synthesis and Characterization of 2, 8 Diazaperylene- 1,3, 7-9-tetraone, a new Anthracene diimide containing Six-member-Imide rings. Organic Letters, Vol.13, Number 10, pp 2560-2563.

Muthu S., Rajamani T., Karabacak M., Asiri A. M. (2014). Vibrational and UV Spectra, First Order Hyperpolarizability, NBO, and HOMO-LUMO analysis of 4-Chloro-N-(2-Methyl- 2-3-dihydroindol-1-yl)-3-Sulfamoyl Benzamide. Spectrochimica Acta Part A. *Molecular and Biomolecular Spectroscopy, 122, pp1-14.*

Nobel N. K. Bamba K. Patrice O. W. Ziao N. (2017). Natural Bond Orbital Population Analysis and Electronic Calculation of Four Azopyridine Ruthenium Complexes by DFT Method. Computational Chemistry, 5, pp 51-64.

Numi K. Hiroki M. Eigo M. Itaru O. Hayato K. Kazuo T. Chihaya A.(2012).[2, 2'] Bi[[naphtha[2,3-6]Furanyl]; A Versatile Organic Semiconductor with a Furan-Furan junction. Chemical

DOI: 10.56892/bima.v8i1.636

Communication, 48, pp 5892-5894. The Royal Society of Chemistry.

O'Boyle N. M., Tenderholt A. L., and Langner K. M."Cclib (2008): A Library for Package- Independent Computational Chemistry Algorithms," *Journal of Computational Chemistry*, Vol. 29, no. 5, pp839–845.

Raghunath P. Ananth M. R. Gouri C. Bhanuprakah K. Jayathirtha V. R. (2006). Electronic Properties of Anthracene Derivatives for Blue light emitting Electroluminescent layers in Organic LEDs. A DFT Study. Journal Physical Chemistry, 110, pp 1152-1162.

Reis H. Papadopoulos M. G. Munn R. W. (1998). Calculation of Macroscopic first, second and third-order Optical Susceptibilities for the urea Crystal. Journal of Chemical Physics, Vol.109, Number 16, pp 6828-6838.

Runge E. and Gross E. K. U. (1984). Density Functional Theory for Time-Dependent Systems. *Physics Review Letters, 52, pp997-1000*

Sam-Shajiing S. Larry R. D. (2017). Introduction to Organic Electronics and Optoelectronic Materials and Devices. 2nd Edition, CRC Press.

Tyson D. S, Ashley D. C, Faysal I, Javier S. P, Michael A. M,(2008). Novel Anthracene Diimide Fluorescent Sensor. Chemical Material, Vol.20, Number 21, pp 6595-6596.

Usta A., Choongik K., Zhiming W., Shaofeng L. Hui H. Faccehetti A. Tobin J.M. (2012). ADI- Based Semiconductor for Air-Stable, n-channel Organic Thin-Film Transistors; Material Design, Synthesis and Characterization. Journal of Material Chemistry, Vol. 22, pp 4459-4472.

Wang C. Huanli D. Wenping H. Yungi L. Daoben Z.(2012). Semiconducting π -conjugated systems in Field Effect Transistors. A material Odyssey of Organic Electronic. Chemical Reviews, 112, pp 2208-2267. American chemical society.

Wang Z. Kim C. Faccehetti A. Mark T. J. (2007). Journal American Chemical Society, 129, pp 13362

Yin J. Chaitanya K. and Ju X. H. (2016). Bromination and Cyanation for improving Electron Transport Performance of Anthra-tetrathiophene. Journal of Material Resources. Vol.31, Number 3, pp 337-347.

Yon D. Wang H. Du B.(2010). Introduction to Organic Semiconductor Heterojunctions Singapore, John Wiley and Sons Inc.

Yongfang L. (2015). Organic Optoelectronic materials. Lecture Notes in Chemistry, Vol. 91. Springer. DOI; 10.1007/978-3-319-16862-3.